Dan - final ver (after referees comments)
FYI
Bill

Site-selective spectroscopy in dysprosium-doped chalcogenide glasses for 1.3μm optical fibre amplifiers

T. Schweizer, F. Goutaland†, E. Martins*, D.W. Hewak, and W.S. Brocklesby

Optoelectronics Research Centre, University of Southampton, Southampton SO17 1BJ, UK

†present address: Laboratoire TSI, 23, rue du Dr. P. Michelon, 42023 St Etienne cedex 2, France

** present address: Infineon Technologies, Otto-Hahn-Ring 6, 81739 Munich, Germany*

Abstract:

Dy^{3+}-doped chalcogenide glasses are potential candidates for 1.3μm optical fibre amplifiers. This paper describes spectroscopic characterization of Dy^{3+}-doped gallium lanthanum sulphide glasses with low and high oxide content (GLS and GLSO). The spectroscopic investigations show that small amounts of oxide (~1%) in GLS sulphide glass create a second group of sites with a different local environment to that of the main sulphide sites. Dy^{3+} ions in the oxide site, which can constitute up to ~1/3rd of the total number of Dy^{3+} ions, experience a high phonon energy environment and do not show any 1.3μm emission and hence cannot provide gain for a potential 1.3 μm optical fibre amplifier in this material.

Introduction

Recently Dy^{3+}-doped chalcogenide glasses attracted much interest for their potential application as a 1.3 μm optical fibre amplifier for telecommunications (Fig. 1) [1, 2, 3, 4]. The 1.3 μm level, which is completely quenched in fluoride and oxide glasses due to strong multiphonon decay across the small energy gap of 1850 cm^{-1} to the next lower level, has a radiative quantum efficiency of 19% in gallium lanthanum sulphide (GLS) glass [4]. Based on this value even higher quantum efficiencies are expected for the $^6H_{11/2}$ and $^6H_{13/2}$ levels which have larger energy gaps to the next lower level (Fig. 1). Indeed 1.8, 2.9, and 4.3 μm emissions have been reported from Dy^{3+}-doped chalcogenide glasses [5, 6, 7, 8, 9]. General spectroscopic information about the 1.3 μm transition in GLS including a Judd-Ofelt analysis can be found in [3, 4, 10].

The following paper presents some new spectroscopic results which improve our understanding of the Dy:GLS glass system and of its suitability as a material for a 1.3 μm fibre amplifier. The experiments clearly revealed that about one third of the Dy^{3+} ions experience a high-phonon-energy environment that would not normally be expected in a low-phonon-energy chalcogenide glass such as GLS ($70Ga_2S_3$:$29La_2S_3$:$1La_2O_3$). (This again shows that GLS glasses, previously believed to be pure chalcogenides, have small levels of oxides, which provide a second site for rare earth dopants.) The paper is divided into two parts. Part I describes the spectroscopic properties of Dy^{3+}-doped GLS glass with respect to the existence of two very distinct groups of sites in the glass and compares this to the spectroscopy of Dy^{3+}-doped GLSO glass ($70Ga_2S_3$:$30La_2O_3$). In Part II we use Raman measurements on the GLS and GLSO host glasses to attempt to relate the structure of the La site as indicated from Raman to the observed Dy^{3+} spectroscopy.

PART I

Site selectivity in Dy^{3+}-doped GLS glass

We have fabricated GLS glass samples by melting high purity raw materials, gallium sulphide, lanthanum sulphide and lanthanum oxide, in a vitreous carbon crucible at 1150°C. Melting was performed in a tube furnace with flowing dry argon. This ensured that samples were of the high purity, with no detectable OH- in the final glass. Oxide impurities were carefully monitored in the precursors by a LECO analysis and in the final glass by infrared spectroscopy.

Recently, our understanding of vitrification in the GLS glass family has improved and the key role that oxides play in glass formation is now understood [11]. Early work on GLS glasses failed to recognize that a small percentage, typically 2% by weight, of lanthanum oxide is required to form a glass. In the past, when glasses were realized, impurity levels of oxides in the raw materials were sufficiently high that glass formation was favoured. Without this oxide, whether added intentionally or as an impurity in the precursors, crystallization of the glass is a problem and glass formation is hindered. As a result, spectroscopic work presented on pure sulphide was in reality being performed on glasses with significant quantities of oxide.

The Dy^{3+} absorption bands show an unusual double structure in GLS glass (Fig. 2.a). The absorption bands at 760, 810, and 910 nm are each accompanied by a smaller absorption peak at 740, 790, and 880 nm. The 1.1 and 1.3 μm bands have a shoulder at their short-wavelength side while this particular structure is not obvious for the 1.7 and 2.8 μm bands. The fact that the absorption bands at 810 nm, 910 nm, 1.1 μm, and 1.3 μm are all comprised of two energy levels (Fig. 1) offers a possible explanation for the double structure. However, the double

structure is not apparent in the absorption spectra of other glasses [1, 2, 12, 13, 14] and in high oxide GLS glass (GLSO) (Fig. 2.b).

The measurement of excitation spectra revealed an interesting explanation for the origin of the double structure. For these experiments the Dy^{3+}-doped glass samples were excited with a tuneable Ti:sapphire laser. The Dy^{3+} fluorescence was collected with a set of two CaF_2 lenses, imaged through a 300-mm monochromator onto a nitrogen cooled InSb detector. Excitation spectra of the 1.3, 1.8, and 2.9 μm emission bands (see Fig. 1) were measured by setting the monochromator to the respective emission wavelength and tuning the Ti:sapphire pump wavelength from 720-850 nm and 830-970 nm while monitoring the intensity of the fluorescence signals at each of the three emission wavelengths for a constant pump power. Fig. 3 shows the excitation spectra of the 1.3 μm and 2.9 μm emission bands along with a Dy^{3+} absorption spectrum in the 720-970 nm pump wavelengths region. (The excitation spectrum for the 1.8 μm emission is not shown and is similar to that of the 1.3 μm emission.) Clearly the excitation spectra do not follow the absorption spectrum. Pumping into the short-wavelength absorption peaks generates hardly any fluorescence at 1.3 μm and 2.9 μm.

This result suggests the existence of two different types of Dy^{3+} sites, each of which has a statistical distribution of different sites leading to the inhomogeneous line broadening observed in glasses. Dy^{3+} ions in one of the two types of sites absorb at slightly shorter wavelength and either show very weak fluorescence or no fluorescence at all. A very similar effect, though less pronounced, has been reported by our group in Pr^{3+}-doped GLS glass [15]. The authors concluded that oxide impurities in the glass lead to a second, more favourable Pr^{3+} site which absorbs at shorter wavelength than the sulphide site and also shows a reduced fluorescence decay time due to locally increased multiphonon decay rates for ions in the oxide site. At that time however, the key role of oxygen in glass formation was not understood.

The reasoning for two sites with different phonon energies can be applied to Dy^{3+}-doped GLS and is supported by (i) the small difference of the 1.3 and 2.9 μm excitation spectra, (ii) the pump wavelength dependent fluorescence spectra, and (iii) pump wavelength dependent lifetime measurements. The comparison of these results with the spectroscopy of Dy^{3+}-doped GLS glasses with 30mol% La_2O_3 content (GLSO glass) gives evidence that the high phonon energy site in GLS is caused by the addition of 1% La_2O_3. Since the site with the higher phonon energy is likely to be related to an oxide environment it will be referred to in this paper as the "oxide site" whereas the low phonon energy site will be referred to as the "sulphide site". Assuming similar absorption cross sections for the ions in the two sites we can estimate from the strength of the two absorption peaks that about one third of all Dy^{3+} ions sit in the oxide site whereas two thirds sit in the sulphide site (Fig. 2). The three sets of experiments that support the existence of an oxide site in low oxide GLS will now be described.

(i) Excitation spectra

As mentioned above, fluorescence intensities are very low when pumping the short wavelength peak of the absorption bands, indicating that the double structure in the absorption spectrum is caused by two groups of Dy^{3+} sites with different spectroscopic properties. Fluorescence from the Dy^{3+} ions that absorb at shorter wavelengths seems to be quenched by non-radiative multiphonon decay. The rate of the multiphonon decay, which can shorten the lifetime of the energy levels, depends exponentially on the size of the energy gap to the next lower lying level and on the maximum phonon energy of the surrounding glass matrix [1, 12]. The 2.9 μm level ($^6H_{13/2}$) has a larger energy gap to the ground state than the 1.3 μm level ($^6H_{9/2}$,$^6F_{11/2}$) has to the level below it (Fig. 1) and should therefore have lower multiphonon decay rates in both sites. Indeed some 2.9 μm emission was measured for 740, 790, and

880 nm pumping (Fig. 3) indicating that emission can be obtained from the oxide site from levels with an energy gap to the next lower level that is sufficiently large to prevent complete quenching. The difference between the 1.3 μm and the 2.9 μm excitation spectra therefore supports the idea that the two different classes of Dy^{3+} sites have a local environment with different maximum phonon energies. This model is depicted in Fig. 4 that shows some of the radiative and non-radiative transitions for the two sites. Higher non-radiative transition rates for ions in the oxide site as indicated by the dashed arrows, quench the 1.3, 1.8, and 4.3 μm emission and decrease the intensity of the 2.9 μm emission.

(ii) Fluorescence spectra

To further support the idea of two classes of sites we investigated the pump wavelength dependence of the 2.9 μm fluorescence spectrum in GLS glass and compared this to the same emission coming from Dy^{3+}-doped GLSO glass. Other emission bands cannot be compared since they are quenched for ions in the oxide site.

The fluorescence spectra were measured with the same set-up used for the excitation experiment described above. The spectra were corrected for the system response (detector, monochromator, water absorption in air, etc.) using a black body radiation source.

The similarity between the shape of the emission spectra from ions in the high phonon energy site in low oxide GLS glass and ions in GLSO glass (Fig. 5) give further evidence that the high phonon energy site is actually caused by an oxide environment.

(iii) Lifetime measurements

The model of two classes of sites with different phonon energies is further supported by lifetime measurements. As for the fluorescence measurements, the lifetime measurements focus on the fluorescence decay of the 2.9 μm transition since all other transitions are

quenched for ions in the oxide site. The fluorescence decay time of the 2.9 μm transition is expected to be shorter for ions in the oxide site due to competing multiphonon decay.

As before the Dy^{3+} ions were excited with a tuneable Ti:sapphire laser. The laser beam was modulated using a mechanical chopper in the focal plane between two x10 microscope objectives. The fluorescence was imaged onto the InSb detector through a 2.54 μm long-wavelength-pass filter. The signal was averaged with a digital storage oscilloscope. The time response of the system was better than 10 μs.

Fig. 6 shows three fluorescence decay curves for the 2.9-μm Dy^{3+} transition. In low oxide GLS the decay follows a single exponential with a 1/e lifetime of 2.75 ms for a pump wavelength of 910 nm. Tuning the pump laser to 875 nm leads to a new feature in the decay curve. The decay now starts with a fast exponential decay of about 200 μs and then follows the decay for 910 nm pumping. The fast component of the decay is in the same order of the decay curve found in GLSO glass (1/e about 100 μs). This reinforces the theory that by tuning to the short-wavelength absorption peak we excite Dy^{3+} ions with a high phonon environment, probably a mixed oxide-sulphide environment.

Based on these three sets of experiments we can conclude that GLS glasses contain oxide impurities that provide an oxide environment for about one third of the Dy^{3+} ions. Dy^{3+} ions in the oxide site have higher multiphonon rates which either lead to decreased fluorescence decay times, as for the 2.9 μm emission, or to complete fluorescence quenching, as for the 1.3 and 1.8 μm emissions. Ions in these sites also show a different Stark splitting and a different nephelauxetic effect leading to a change in the shape of the emission spectra. The smaller nephelauxetic effect, i.e. the lower local refractive index for ions in the oxide site shifts the

energy levels to higher energies compared to the ions in the sulphide site, which is reflected by the shorter wavelengths absorption peaks for the ions in the oxide site (Fig. 2).

PART II

Raman measurements of GLS and GLSO glasses

Raman spectroscopy is a powerful experimental technique used to investigate the structural arrangement of glasses and has been widely used to study several types of chalcogenide glasses [16, 17]. Since the concentration of Dy^{3+} ions in our samples is low ($\leq$ 1.5 mol%) it is not possible to obtain direct information about their local environments in the different glasses. Therefore, we will rather use Raman spectroscopy to understand the chemical arrangement of the glasses and the different solubility mechanisms of the La^{3+} ions. According to the similarities between Dy^{3+} and La^{3+} ions (electronic structure, size), we would expect that these two ions are dissolved through the same chemical pathways into the glasses. We will compare the model of the La site to the local environment of the Dy^{3+} ion, as deduced from fluorescence and absorption spectroscopy.

Raman spectra were recorded at room temperature from 80 to 1000 cm^{-1} with a resolution of 2 cm^{-1} using the 632.8-nm line of a HeNe laser. In order to reduce the effects of thermal population on the intensities of the different Raman vibration modes, we calculated the reduced Raman spectra for each of the samples.

The Raman spectra of the two different samples are divided into two parts: the low energy part, between 80 and 500 cm^{-1}, and the high-energy region, between 450 and 1000 cm^{-1}. The low energy spectra for the GLS and GLSO glasses are presented in Fig. 7.a. Two main bands are observed at 150 and 340 cm^{-1}. The two bands located at 150 and 340 cm^{-1} are identical for

the GLS and GLSO glasses. In the high-energy region, shown in Fig. 7.b, the GLS Raman spectrum shows only a weak broad band, centred around 760 cm^{-1}. In case of the GLSO, two main vibrations can be distinguished at 517 and 640 cm^{-1} but the 760 cm^{-1} vibration is no longer present.

The bands centred at 150 and 340 cm^{-1} have been reported in other Ga-containing chalcogenide glasses and are attributed to asymmetrical bending (ν_4) and symmetrical stretching (ν_1) vibrations of GaS_4 tetrahedra, respectively [18].

GaS_4 tetrahedra, which are the main glass former units, are formed from the reaction of Ga_2S_3 crystal with the sulphur anions (S^{2-}) brought by the addition of La_2S_3 [19]. These sulphur ions break the Ga->S dative bonds characteristic of the crystalline phase, and some GaS_4 tetrahedra with a negative charge are then formed (Fig. 8.a). These negative ionic cavities form some reception sites for the La^{3+} ions, which act as charge compensators for these negative charges. The La^{3+} ions entering the glass through this mechanism are thus expected to have a sulphide environment, because of the GaS_4 tetrahedra surrounding.

The very weak 760 cm^{-1} vibration in GLS glass is attributed to "strained" Ga-related tetrahedra, containing at least one threefold-coordinated oxygen atom linked to three tetrahedra [20]. La^{3+} ions can thus be dissolved into the glass close to these negative charges and act again as charge compensators. The La^{3+} ions dissolved into the glass through this chemical pathway have therefore an oxide-like surrounding because of the threefold-coordinated oxygen atoms.

Consequently, for the GLS sample, there are two different mechanisms for La^{3+} ion incorporation leading to either sulphide or oxide environments for the rare earth ions, thus explaining the double site distribution observed through the luminescence results presented in Part I of this paper.

When the La_2S_3 in GLS is substituted by La_2O_3 to form GLSO, the surrounding of the rare earth ion changes as shown by the luminescence measurements (Part I). Simultaneously, we observe changes in the high-energy part of the Raman spectrum (Fig. 7.b). It has already been reported in other chalcogenide glasses that the behaviour of La_2O_3 in glass formation mechanisms depends strongly on the La_2O_3 concentration [21]. In case of high concentration (case of GLSO), La_2O_3 is expected to act as a network modifier and not only as a charge compensator. The structure of the GLSO glass is thus expected to be close to the GLS one, with Ga-related tetrahedra as the main glass forming units. Similarities between the structures of GLS glasses containing either sulphide or oxide modifiers have been reported previously [22]. Because of the similarities of the electronic structure of oxygen and sulphur ions, we assume the same chemical reaction as the reaction (1) but with O^{2-} replacing S^{2-} anions (Fig. 8.b). Therefore, some Ga-related tetrahedra, with a negative charge, containing both oxygen and sulphur atoms are formed through this mechanism. The two Raman bands centred at 517 and 640 cm^{-1} are attributed to Ga-O-Ga and Ga-O^- bonds, respectively [20, 23], and confirm the formation of gallium-oxygen bonds. Consequently, La^{3+} ions are incorporated in the GLSO glass close to the Ga-related tetrahedra and compensate their negative charges. Compared to the GLS glass, there is only one way for La^{3+} ions to be dissolved into the oxide host matrix, which explains why we observed mostly one kind of site for the Dy^{3+} ions in this glass.

The presence of non-bridging oxygen atoms in the GLSO sample, identified by their characteristic Raman vibration centred at 640 cm^{-1}, shows the efficiency of La^{3+} as network modifier. Non-bridging oxygen atoms formation, through the breaking of Ga-O-Ga units by La^{3+} ions [17], requires therefore the presence of many of these Ga-O-Ga units and thus a very efficient reaction (2). On the contrary, no Raman bands located around 375 cm^{-1} and characteristic of non-bridging-sulphur atoms [24] have been observed. Reaction (1) seems

therefore less efficient than reaction (2). Moreover, a careful examination of the low energy part of the Raman spectra revealed the presence of a weak band centred at 233 cm^{-1}, existing only in case of the GLS sample (Fig. 7a). The subtraction of the spectra for GLS and GLSO allows this band to be distinguished more clearly. Fig. 9 shows the difference between the GLS and GLSO Raman spectra along with the Raman spectrum of Ga_2S_3 crystals.

The 233 cm^{-1} Raman vibration has been reported to be characteristic of Ga_2S_3 crystals and to disappear when the glass is formed as reported previously for GLS [25]. Consequently, its presence in the Raman spectrum of our GLS glasses shows that some structures similar to Ga_2S_3 crystals remain in the glass, indicating again the low efficiency of reaction (1). The number of sulphide reception sites offered to La^{3+} ions through this reaction will therefore be small, explaining why many La^{3+} (and Dy^{3+}) ions will prefer to act as charge compensator for the strained Ga-related tetrahedra, thus having an oxide environment.

Finally, it should be noticed that our Raman spectra did not show any Raman bands related to La-S or La-O bonds, which have been observed in other chalcogenide glasses at 220 and between 300 and 400 cm^{-1} respectively [26, 27]. This has to be related to the very intense and broad ν_1 and ν_4 Raman vibrations, which overlap the La-S and La-O bands.

We can draw three major conclusions from the Raman measurements: (1) The 760 cm^{-1} vibration in the Raman spectrum of GLS glass shows the presence of oxygen in the form of GaO_4^- tetrahedra, (2) the existence of GaO_4^- and GaS_4^- tetrahedra in GLS glass creates two different reception sites for the rare earth ions, and (3) the number of rare earth ions with an oxide environment is high despite the low oxide concentration in GLS glass because of the low efficiency of the reaction forming GaS_4^- tetraheda.

Conclusion

The Dy^{3+}-doped GLS glass system offers a unique opportunity to study the phenomenon of site-selectivity in a glass host. Despite the strong inhomogeneous broadening found in a glass, the two groups of Dy^{3+} ions can clearly be distinguished by absorption, fluorescence, lifetime, and excitation spectroscopy. Comparison of the spectroscopic properties of the two groups of ions with the spectroscopy of Dy^{3+}-doped GLSO glass with only one group of ions gives evidence that the Dy^{3+} ions which give rise to the shorter wavelength absorption peaks experience some kind of oxide environment. This environment could be characterised by Ga-O bonds that give rise to the 760 cm^{-1} phonon energy band in the Raman spectrum of low oxide GLS glass. Although the ratio of oxygen to sulphur in this glass is much lower that 1:2, one third of the Dy^{3+} ions occupy oxide sites. This could be explained by the solubility mechanism, the formation of negative sulphide cavities being less efficient than the formation of oxide cavities as revealed by the Raman spectra. The oxide environment leads to higher multiphonon relaxation rates, which quench the fluorescence from most of the Dy^{3+} energy levels completely, leaving only a weak 2.9 μm emission band. For active devices such as the 1.3 μm optical fibre amplifier it is therefore important to either reduce the oxide contamination of the glass or to carefully select the pump wavelength in order to avoid pumping the ions in the oxide sites. The results also show that high oxide GLS glasses, though easier to pull into fibres, are not a suitable alternative to low oxide GLS glasses for applications relying upon radiative transitions of Dy^{3+} ions.

Acknowledgement

Thanks to Mr. Ben Hudson for glass fabrication.

References

[1] S. Tanabe, T. Handa, M. Watanabe, T. Hayashi, and N. Soga, "Optical properties of dysprosium-doped low-phonon-energy glasses for a potential 1.3 μm optical amplifier," J Am. Ceram. Soc. **78**, 2917-2922 (1995)

[2] K. Wei, D.P. Machewirth, J. Wenzel, E. Snitzer, and G.H. Sigel, Jr., "Spectroscopy of Dy^{3+} in Ge-Ga-S glass and its suitability for 1.3-μm fiber-optical amplifier applications," Opt. Lett. **19**, 904-906 (1994)

[3] D.W.Hewak, B.N.Samson, J.A.Medeiros-Neto, R.I.Laming, D.N.Payne, "Emission at 1.3 μm from dysprosium-doped Ga:La:S glass," Electron. Lett. **30**, 968-969 (1994)

[4] B.N.Samson, J.A.Medeiros-Neto, R.I.Laming, D.W.Hewak, "Dysprosium doped Ga:La:S glass for an efficient optical fibre amplifier operating at 1.3 μm," Electron. Lett. **30**, 1617-1619 (1994)

[5] L. Brandon Shaw, D. Schaafsma, J. Moon, B. Harbison, J. Sanghera, and I. Aggarwal, "Evaluation of the IR transitions in rare-earth-doped chalcogenide glasses," 1997 OSA Technical Digest Series, Volume 11, Conference on Lasers and Electro-Optics, 18-23 May, 1997, Baltimore, Maryland, page 255, paper CWF48

[6] J. Heo, "Optical characteristics of rare-earth-doped sulphide glasses," J. Mater. Sci. Lett. **14**, 1014-1016 (1995)

[7] J. Heo, W.Y. Cho, and W.J. Chung, "Sensitizing effect of Tm^{3+} on 2.9 μm emission from Dy^{3+}-doped $Ge_{25}Ga_5S_{70}$ glass," J. Non-Cryst. Solids **212**, 151-156 (1997)

[8] T. Schweizer, D.W. Hewak, B.N. Samson, and D.N. Payne, "Spectroscopic data of the 1.8, 2.9, and 4.3 μm transitions in dysprosium-doped Ga:La:S glass", Opt. Lett. **21**, 1594-1596 (1996)

[9] Y. Guimond, J.L. Adam, A.M. Jurdyc, J. Mugnier, B. Jacquier, and X.H. Zhang, "Dy^{3+}-doped stabilized GeGaS glasses for 1.3 μm optical fibre amplifiers", Opt. Mater. 12, 467-471 (1999)

[10] B.N. Samson, T. Schweizer, D.W. Hewak, and R.I. Laming, "Properties of dysprosium doped GaLaS fibre amplifiers operating at 1.3μm", Opt. Lett. **22**, 703-705 (1997)

[11] R.H. Li, D. Furniss, H. Bagshaw, A.B. Seddon, "The decisive role of oxide content in the formation and crystallization of gallium-lanthanum-sulfide glasses", J. Mater. Res. 14 (1999) 2621-2627

[12] J. Heo and Y.B. Shin, "Absorption and mid-infrared emission spectroscopy of Dy^{3+} in Ge-As(or Ga)-S glasses," J. Non-Cryst. Solids **196**, 162-167 (1996)

[13] J.L. Adam, A.D. Docq, and J. Lucas, "Optical transitions of Dy^{3+} ions in fluorozirconate glass," J. Solid State Chem. **75**, 403-412 (1988)

[14] R. Cases, M.A. Chamarro, R. Alcala, and V.D. Rodriguez, "Optical properties of Nd^{3+} and Dy^{3+} ions in ZnF_2-CdF_2 based glasses", J. Lumin. **48 & 49**, 509-514 (1991)

[15] R.S. Brown, W.S. Brocklesby, D.W. Hewak, and B.N. Samson, "The effect of oxide on the spectroscopic properties of the praseodymium 1.3 μm transition in gallium-lanthanum-sulphide glass," J. Lumin. **66&67**, 278-284 (1996)

[16] J. Heo, J. Min Yoon and S.Y. Ryou, "Raman spectroscopic analysis on the solubility mechanism of La^{3+} in GeS_2-Ga_2S_3 glasses," J. Non-Cryst. Solids **110**, 115-123 (1998)

[17] L. G. Hwa, J. G. Shiau and S. P. Szu, "Polarized Raman scattering in lanthanum gallogermanate glasses," J. Non-Cryst. Solids **110**, 55-61 (1999)

[18] G. Lucovsky, J. P. deNeufville and F. L. Galeener, "Study of the optic modes of $Ge_{0.30}S_{0.70}$ glass by infrared and Raman spectrocopy," Phys. Rev. **B9**, 1591-1597 (1974)

[19] S. Benazeth, M. H. Thuilier, A. M. Loizeau-Lozac'h, H. Dexpert, P. Lagarde and J. Flahaut, "An EXAFS structural approach of the lanthanum-gallium-sulfur glasses," J. Non-Cryst. Solids **110**, 89-100 (1989)

[20] C. M. Shaw and J. E. Shelby, "Raman-spectroscopy of barium gallosilicate glasses," Phys. Chem. Glass **32**, 48-54 (1991)

[21] J. T. Kohli and J. E. Shelby, "Formation and properties of rare-earth aluminosilicate glasses," Phys. Chem. Glasses **32**, 67-71 (1991)

[22] A. M. Loizeau-Lozac'h, M. Guitard and J. Flahaut, "Sur une nouvelle famille de combinaisons soufrées, de type "melilite"," Mat. Res. Bull. **8**, 75-86 (1973)

[23] Z. Pan and S. H. Morgan, "Raman spectra and thermal analysis of a new lead-tellurium-germanate glass system," J. Non-Cryst. Solids **210**, 130-135 (1997)

[24] C. Julien, S. Barnier, M. Massot, N. Chbani, X. Cai, A. M. Loizeau-Lozac'h and M. Guitard, "Raman and infrared spectroscopic studies of Ge-Ga-Ag sulphide glasses," Mater. Sci. Eng. **B22**, 191-200 (1994)

[25] J. Flahaut, M. Guitard and A. M. Loizeau-Lozac'h, "Rare earth sulphide and oxysulphide glasses," Glass Technology **24**, 149-156 (1983)

[26] J. M. Jewell, P. L. Higby and I. Aggrawal, "Properties of BaO-R_2O_3-Ga2O3-GeO2 (R=Y, Al, La and Gd) glasses," J. Am. Ceram. Soc. **77** (1994) 697-700

[27] K. Fukumi and S. Sakka, "Raman spectra of binary alkali and alkaline earth gallate crystals and glasses," Phys. Chem. Glass. **29** (1988) 1-8

Figure Captions

Fig. 1 Energy level diagram of lower Dy^{3+} energy levels with a number of radiative (solid arrows) and non-radiative transitions (dashed arrows)

Fig. 2 Absorption spectra of (a) GLS and (b) GLSO glasses each doped with 1.5mol% Dy_2S_3. The insets in each case show an expansion of the near infrared region of the spectrum, from 700nm to 1μm. This expanded spectrum shows clearly the doublet structure in (a), the absorption bands in GLS glass which is not seen in the GLSO glass.

Fig. 3 Excitation spectra of the 1.3 μm and the 2.9 μm emission bands in Dy^{3+}-doped GLS (0.1 mol% Dy_2S_3) glass along with the absorption spectrum. The excitation spectra do not follow the shape of the absorption spectrum. Note the small difference between the two excitation spectra (see text for details).

Fig. 4 Radiative (solid arrows) and non-radiative (dashed arrows) transitions for Dy^{3+} ions in the sulphide site and in the oxide site. Higher non-radiative decay rates for Dy^{3+} ions in the oxide site quench all radiative transitions but the 2.9 μm emission.

Fig. 5 a) Fluorescence spectra of the $^6H_{13/2} \rightarrow {}^6H_{15/2}$ transition in GLS glass for *two different pump wavelengths*. Pumping at 910 nm excites mainly ions in the sulphide sites while pumping at 870 nm excites mainly ions in the oxide site (see Fig. 2).

b) Fluorescence spectra of the $^6H_{13/2} \rightarrow {}^6H_{15/2}$ transition in *two different glasses*, GLS and GLSO pumped at the peak absorption wavelengths, 890 and 910 nm, respectively.

Fig. 6 2.9 μm fluorescence decay curves for GLS glass (0.1 mol% Dy_2S_3) pumped at 875 nm and 910 nm and for GLSO glass (0.05 mol% Dy_2S_3) pumped at 890 nm. Pumping GLS glass at 910 nm mainly excites ions in the sulphide site while pumping

at 875 nm mainly excites ions in the oxide site (fast initial decay) which have a fluorescence decay time in the same order as measured in the GLSO glass.

Fig. 7 a) low-energy region and b) high-energy region of the Raman spectra of GLS (solid line) and GLSO (dotted line) glasses. The spectra in the low-energy part are almost identical while the high-energy part shows more pronounced differences.

Fig. 8 Formation of a) negative "sulphide" cavities (reaction 1, GLS) and b) negative "oxide" cavities (reaction 2, GLSO)

Fig. 9 Difference between the GLS and GLSO Raman spectra (solid line) along with the Raman spectrum of Ga_2S_3 crystals (dotted line). The similarity of the two spectra reveals the presence of crystal-like structures in the GLS glass.

Figure 1

TOP

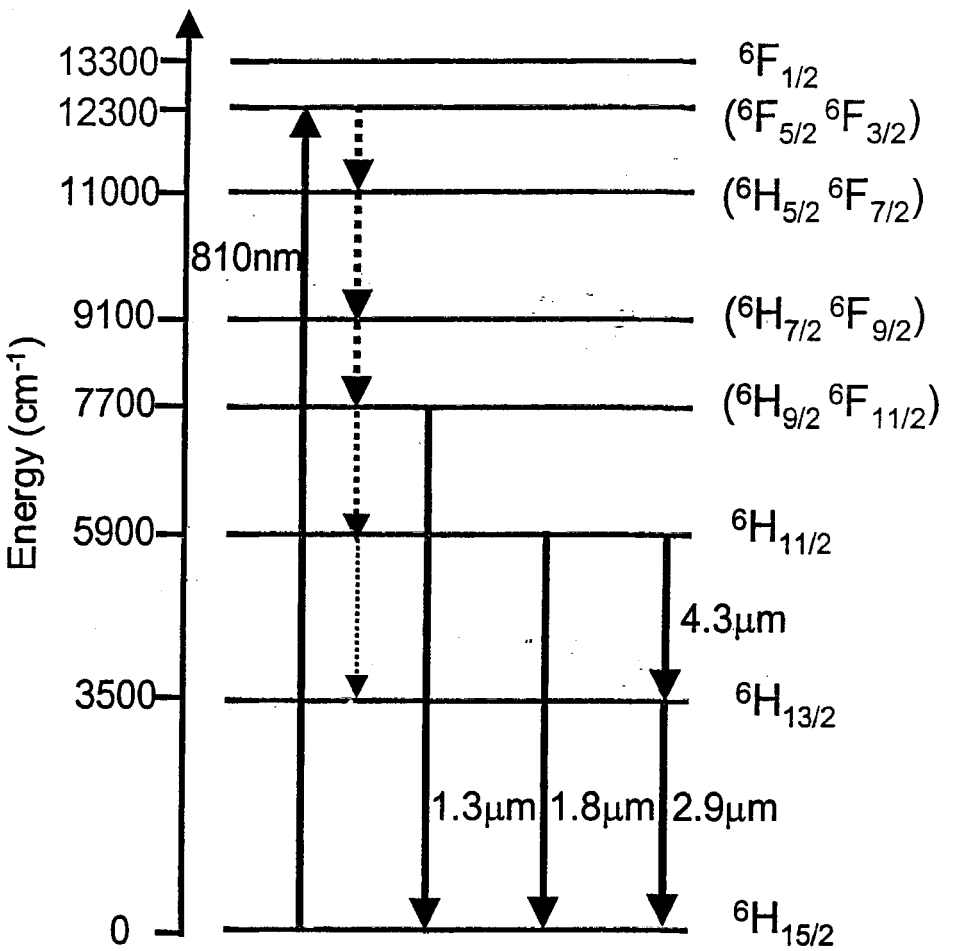
13300
12300
11000
9100
7700
5900
3500
0
Energy (cm-1)
810nm
6F1/2
(6F5/2 6F3/2)
(6H5/2 6F7/2)
(6H7/2 6F9/2)
(6H9/2 6F11/2)
6H11/2
4.3µm
6H13/2
1.3µm
1.8µm
2.9µm
6H15/2

Figure 2

TOP

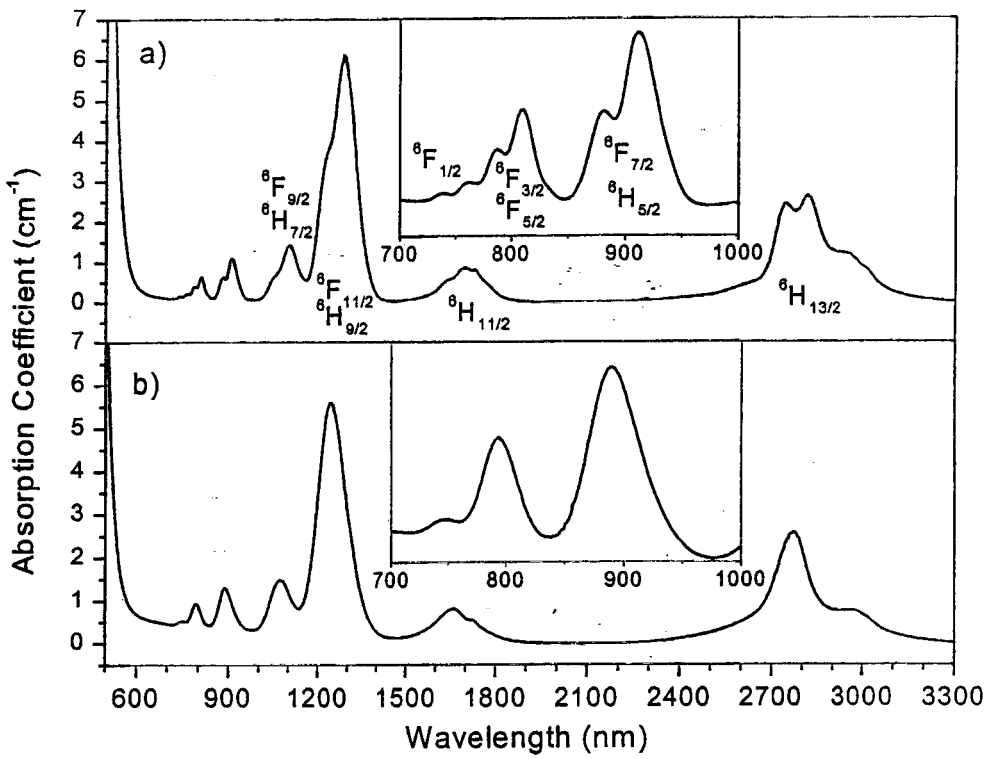
a)
b)
$^6F_{9/2}$
$^6H_{7/2}$
$^6F_{11/2}$
$^6H_{9/2}$
$^6H_{11/2}$
$^6H_{13/2}$
$^6F_{1/2}$
$^6F_{3/2}$
$^6F_{5/2}$
$^6F_{7/2}$
$^6H_{5/2}$
Absorption Coefficient (cm^{-1})
Wavelength (nm)
0 1 2 3 4 5 6 7
600 900 1200 1500 1800 2100 2400 2700 3000 3300
700 800 900 1000

Figure 3

TOP

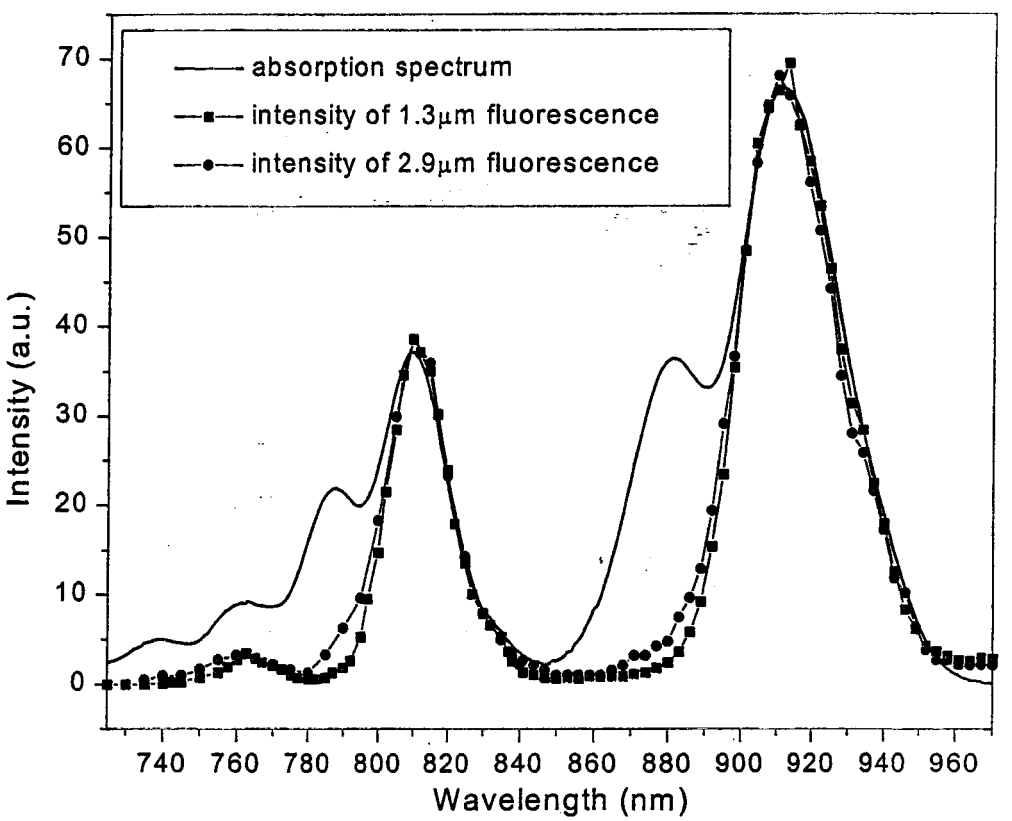
absorption spectrum
intensity of 1.3μm fluorescence
intensity of 2.9μm fluorescence
Intensity (a.u.)
0
10
20
30
40
50
60
70
740
760
780
800
820
840
860
880
900
920
940
960
Wavelength (nm)

Figure 4

TOP

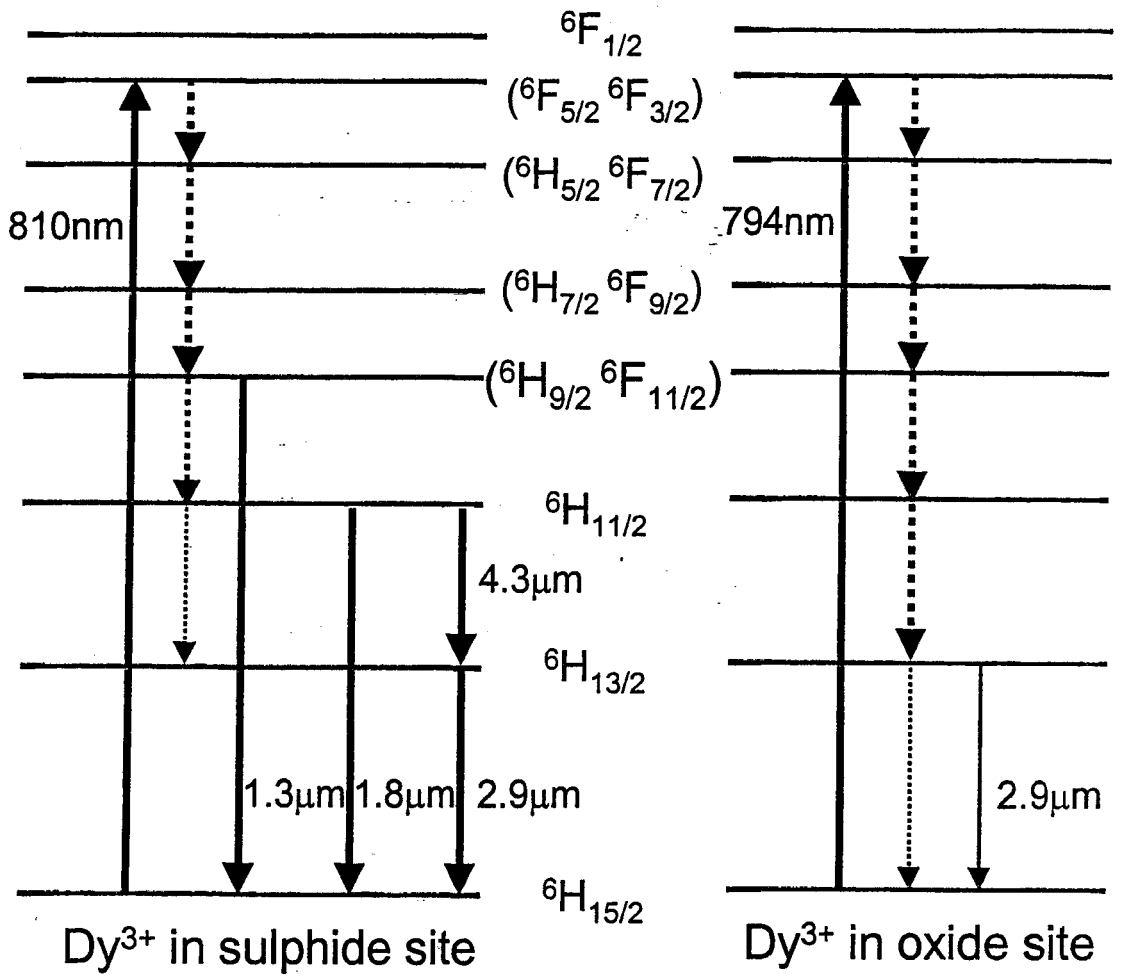
$^6F_{1/2}$
$(^6F_{5/2}\ ^6F_{3/2})$
$(^6H_{5/2}\ ^6F_{7/2})$
810nm
794nm
$(^6H_{7/2}\ ^6F_{9/2})$
$(^6H_{9/2}\ ^6F_{11/2})$
$^6H_{11/2}$
4.3μm
$^6H_{13/2}$
1.3μm
1.8μm
2.9μm
2.9μm
$^6H_{15/2}$
Dy^{3+} in sulphide site
Dy^{3+} in oxide site

Figure 5

TOP

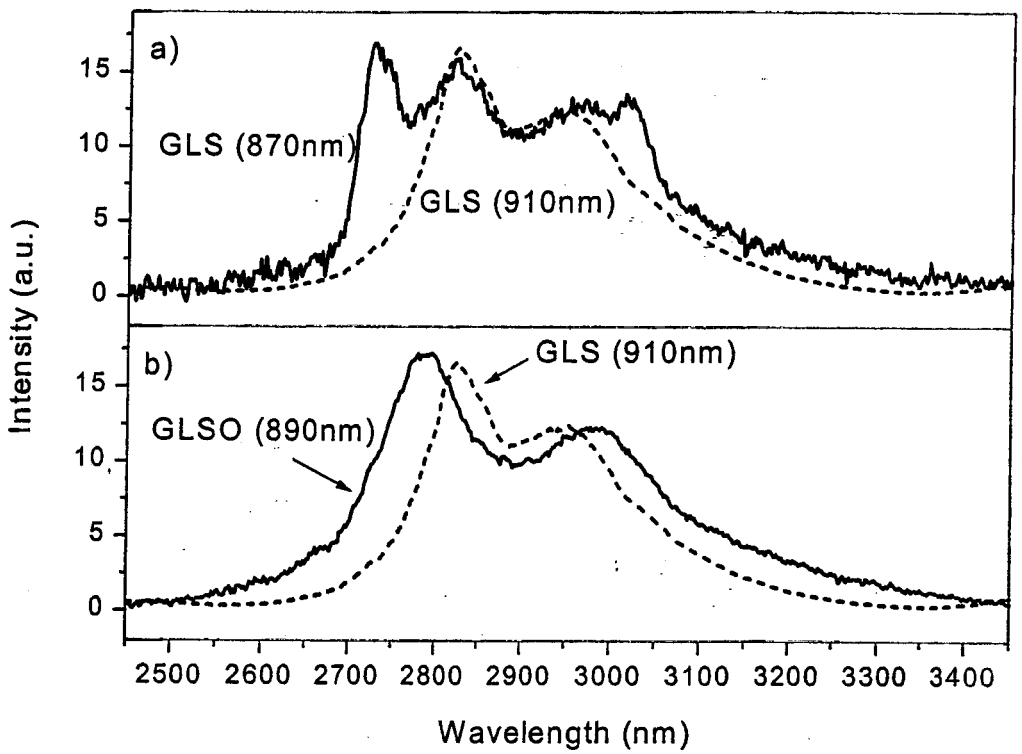
a)
GLS (870nm)
GLS (910nm)
b)
GLS (910nm)
GLSO (890nm)
Intensity (a.u.)
Wavelength (nm)
0
5
10
15
2500
2600
2700
2800
2900
3000
3100
3200
3300
3400

Figure 6

TOP

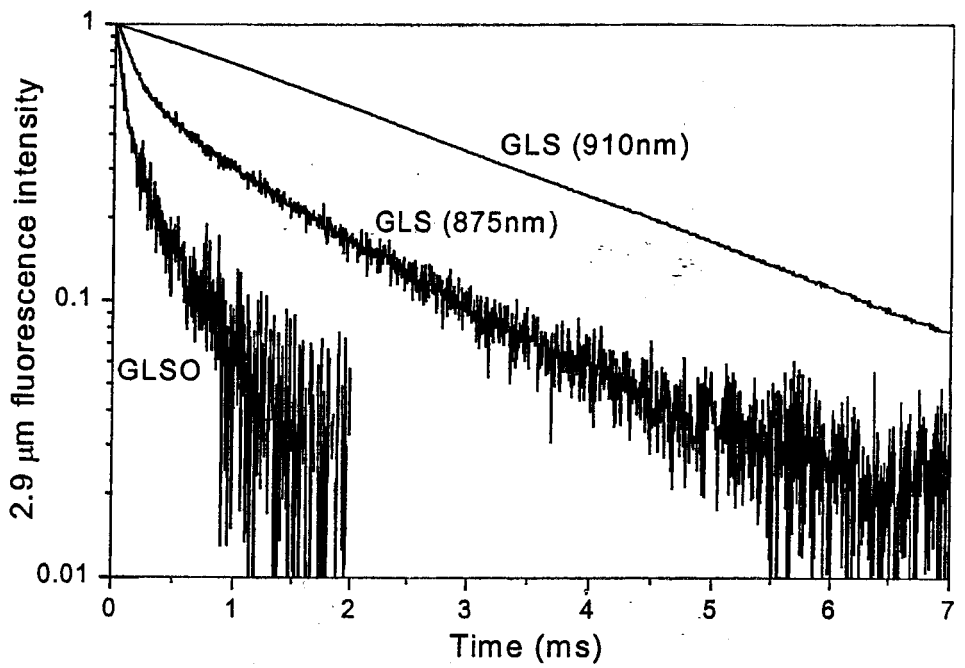
1
0.1
0.01
2.9 μm fluorescence intensity
GLS (910nm)
GLS (875nm)
GLSO
0
1
2
3
4
5
6
7
Time (ms)

Figure 7

TOP

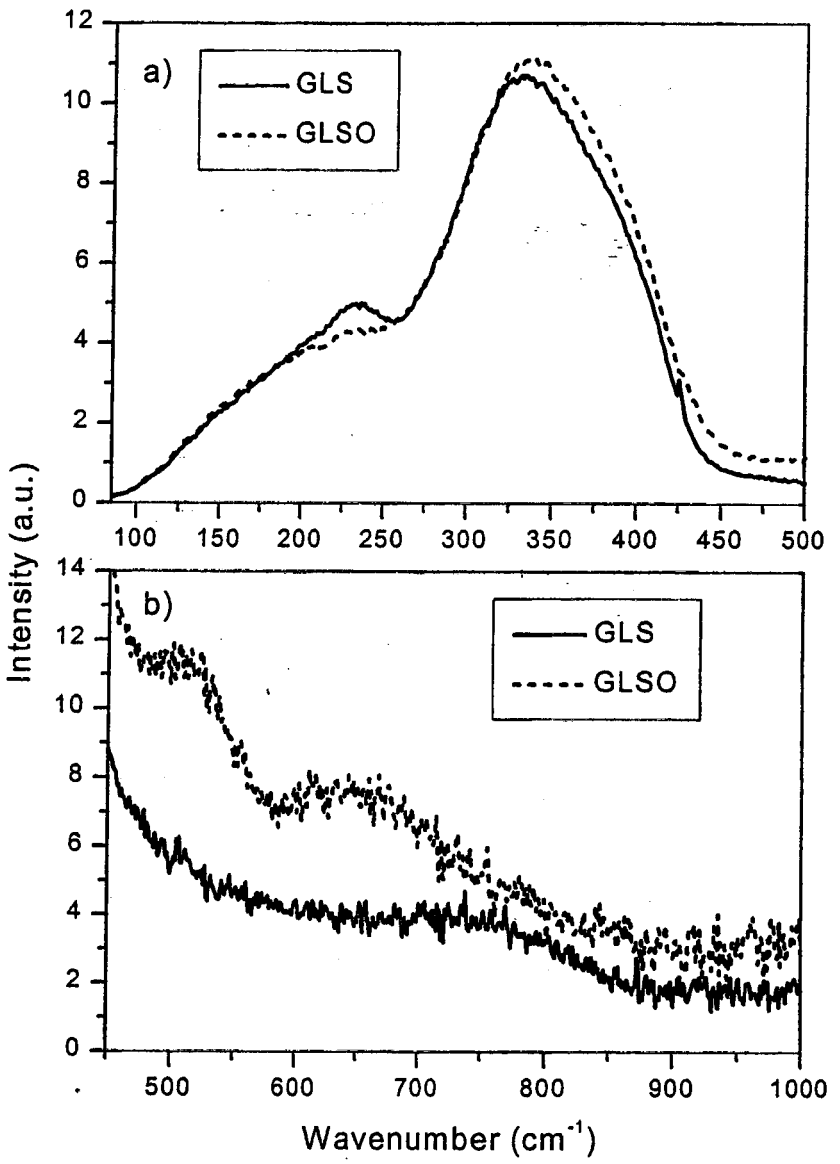

Figure 8

TOP

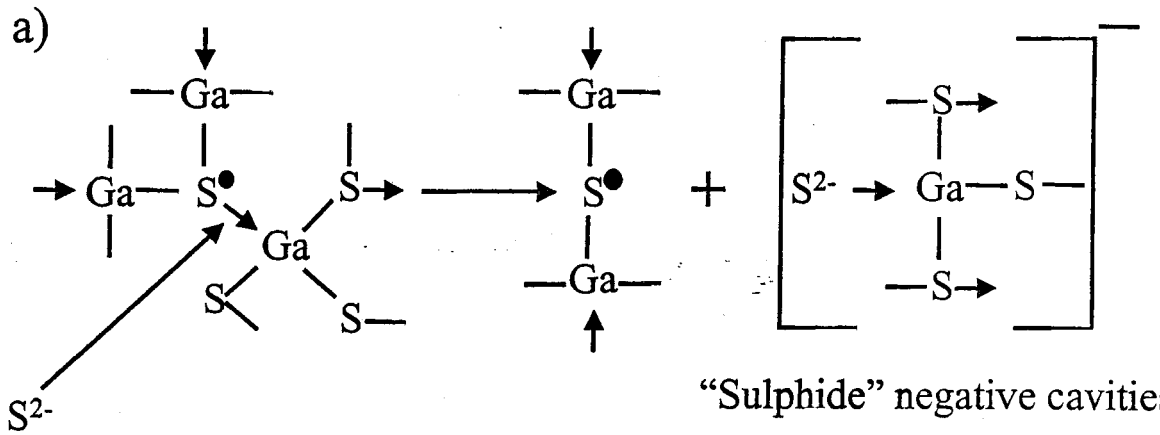

"Sulphide" negative cavities

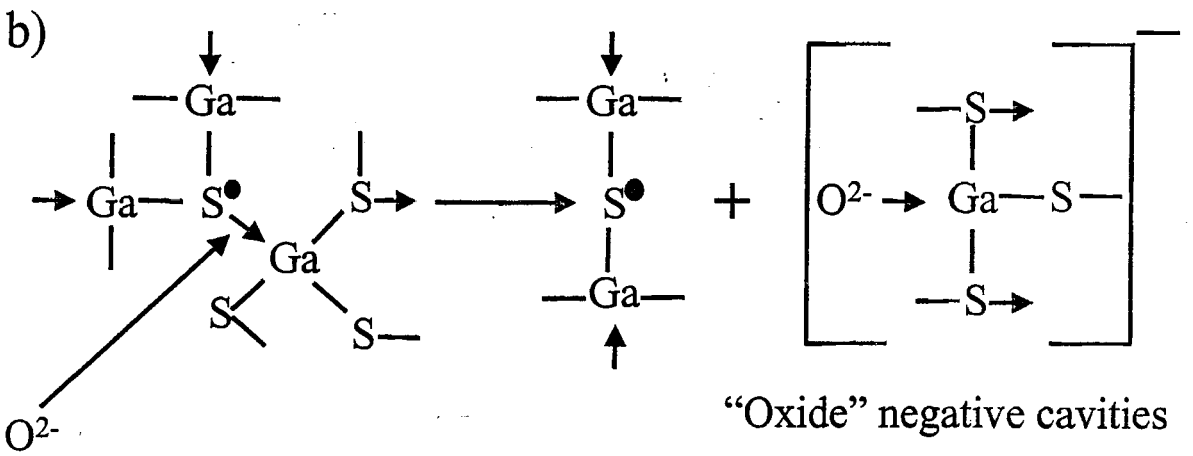

"Oxide" negative cavities

Figure 9

TOP

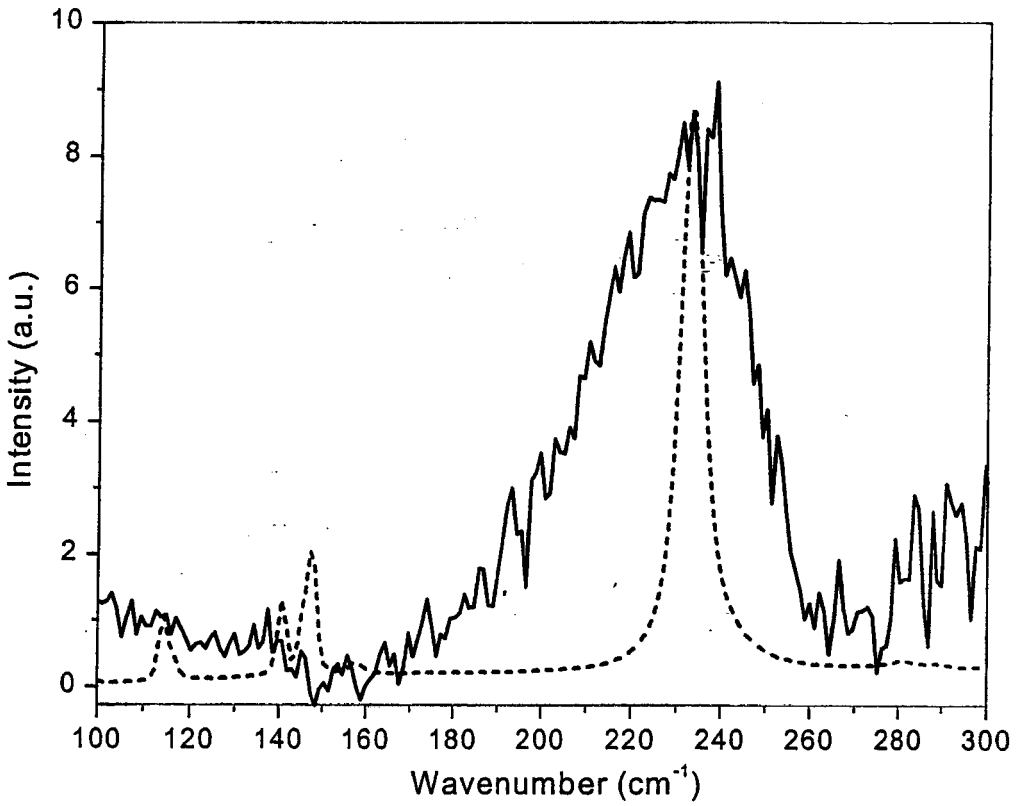
10
8
6
4
2
0
Intensity (a.u.)
100
120
140
160
180
200
220
240
260
280
300
Wavenumber (cm-1)